

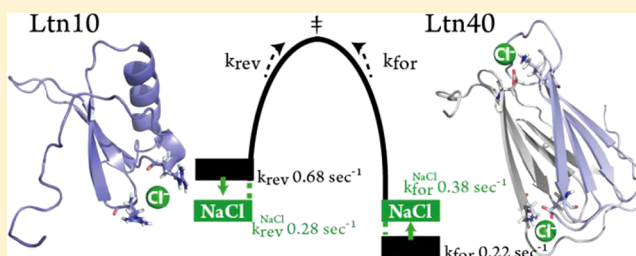
Electrostatic Optimization of the Conformational Energy Landscape in a Metamorphic Protein

Robert C. Tyler, Jamie C. Wieting, Francis C. Peterson, and Brian F. Volkman*

Department of Biochemistry, Medical College of Wisconsin, Milwaukee, Wisconsin 53226, United States

S *Supporting Information*

ABSTRACT: The equilibrium unfolding reaction of Ltn, a metamorphic C-class chemokine, was monitored by tryptophan fluorescence to determine unfolding free energies. Measurements revealed that addition of 150 mM NaCl stabilized the Ltn chemokine fold by approximately 1 kcal/mol. Specific mutations involving Arg23 and Arg43 also increased the stability by 1 kcal/mol, suggesting their involvement in chloride ion coordination. This interaction was confirmed by nuclear magnetic resonance (NMR) salt titration studies that revealed chemical shift perturbations localized to these residues and backbone amides within the proximal 40s loop. The effects of NaCl on the free energy landscape were further verified by ZZ-exchange NMR spectroscopy. Our results suggest that changes in the electrostatic environment modulate the Gibbs free energy of folding and alter the forward and reverse rates of interconversion. These results demonstrate how solution ions can promote metamorphic folding by adjusting the relative stabilities of two unrelated Ltn native-state structures.



The interactions between a protein and its surroundings ultimately define its function, which is encoded in a specific three-dimensional (3D) structure. The consensus view originally proposed by Anfinsen is that a protein adopts a single native-state fold, within the context of its environment, representing a minimum in the Gibbs free energy.¹ This thermodynamic hypothesis implies that a protein's native-state structure is determined solely by its primary sequence and the composition of the surroundings (e.g., pH, solvent, ions, etc.). However, while the vast majority of proteins predictably adopt a single native-state conformation (with varying degrees of flexibility), nothing precludes the existence of primary sequences that populate more than one native-state fold provided their free energies are nearly equal. Interestingly, a small number of naturally occurring proteins have shown the extraordinary ability to actively switch their native-state fold, defining a new category of “metamorphic proteins”.^{2,3}

Of the several examples now documented,⁴⁻⁷ the chemokine lymphotactin (Ltn/XCL1) undergoes one of the most remarkable native-state transformations. In one state, termed Ltn10, the protein adopts the canonical chemokine fold comprised of a three-strand β -sheet and a C-terminal α -helix, which converts into a dimeric β -sheet fold termed Ltn40. Unlike other metamorphic proteins in which a majority of substructure is retained throughout the interconversion process, Ltn native-state transformation requires complete restructuring of all hydrogen bonds and tertiary contacts.⁷ Under near-physiological conditions (37 °C and 150 mM NaCl), both Ltn conformations are equally populated ($K_{eq} \sim 1$), and each is required for proper biological function.⁷

It was revealed early in these studies that the Ltn10–Ltn40 equilibrium could be shifted by adjusting solution conditions.⁸ For instance, with a high salt concentration (200 mM NaCl) and a low temperature (10 °C), the Ltn10 chemokine fold is exclusively populated, while at a high temperature (40 °C) with no salt (0 mM NaCl), the alternate Ltn40 β -strand configuration is strongly favored. Numerous reports have detailed the effects of various salts on protein stability,^{9–11} but the specific role of solution ionic strength in modulating metamorphic interconversion has not been investigated.

Ltn is rich in basic amino acids (nine Arg and six Lys residues; 93 total residues). Because the protein carries a net positive charge, it is likely that electrostatic interactions contribute to the salt dependence of the Ltn10 conformation. In fact, replacement of Arg23 and/or Arg43 with alanine led to an increase in the Ltn10 population relative to the Ltn40 population, even in the absence of salt.¹² Given the proximity of positively charged Arg23 and Arg43 side chains in Ltn10 (~10 Å), which are separated by ~20 Å in Ltn40, we speculated that electrostatic repulsion selectively destabilizes the chemokine fold.¹² Conversely, Ltn40 contains two potential salt bridges, from Arg9 to Asp50 (intramolecular) and from Lys25 to Glu31 (intermolecular), which may be weakened by the addition of salt. Interestingly, a molecular dynamics (MD) simulation that investigated the effect of salt concentration on Ltn10 structural stability revealed a chloride ion persistently associated with the

Received: June 22, 2012

Revised: October 25, 2012

Published: October 26, 2012

Arg23 and Arg43 side chains as well as backbone amides within the 40s loop.¹³ Collectively, these observations suggest that Coulombic forces contribute to metamorphic rearrangements in Ltn. However, the effects of salt on the Ltn10–Ltn40 equilibrium have not been quantified, and the participating structural elements remain undefined. Here we use a combination of equilibrium unfolding, NMR binding, and kinetic-exchange measurements to quantify the changes in Ltn free energy associated with a more ionic environment and mutation. Our results indicate that interactions between Arg23 and Arg43 have a destabilizing effect on the Ltn10 free energy that can be overcome by increasing the ionic strength of the surroundings. This effect is further corroborated by kinetic analysis, revealing that ionic environments beneficial to Ltn10 will destabilize the Ltn40 structure. The consequence of electrostatic tuning of the Ltn free energy is discussed in the context of other metamorphic proteins.

MATERIALS AND METHODS

Protein Expression, Purification, and Mutagenesis. All proteins were expressed and purified using established protocols that have been previously reported.¹⁴ All mutant Ltn proteins were produced by employing the QuickChange site-directed mutagenesis kit following the manufacturer's instructions, with no deviation in expression or purification protocols.

Equilibrium Unfolding Experiments and Determination of Unfolding Free Energies. Experimental measurements were performed on a Photon Technology International (PTI) spectrofluorometer in a fluorescence cuvette with a 1 cm path length equipped with a stir bar rotating at 240 rpm. An excitation wavelength of 283 nm was used with a bandwidth of 4 nm. The fluorescence emission for WT Ltn was collected between 310 and 360 nm ($\lambda_{\text{max}} = 332$ nm) recorded at 1 nm increments with a signal acquired for 2 s at each wavelength employing a 6 nm bandwidth. Fluorescence emission spectra for the mutant proteins were collected with identical parameters and all displayed a λ_{max} of 332 ± 1 nm. Fresh urea stocks were used for all unfolding measurements following standard laboratory practices.¹⁵ All data points in the unfolding curve were determined with a separate solution containing 5 μM protein in 20 mM Na_2HPO_4 (pH 6). Unfolding curves were recorded by monitoring the fluorescence intensity at 332 nm as a function of urea concentration. The free energy of each point in the unfolding transition zone was determined from the equation

$$\Delta G_u = -RT \ln(K_u) \quad (1)$$

where K_u is the equilibrium unfolding value at each urea concentration. K_u was determined using a two-state unfolding model based on the equation

$$K_u(\text{urea}) = \frac{Y_f - Y_{\text{urea}}}{Y_{\text{urea}} - Y_u} \quad (2)$$

where Y_f and Y_u represent the folded and unfolded baselines, respectively, and Y_{urea} represents the fluorescence signal as a function of urea concentration. The final ΔG_{unfold} value was obtained by extrapolation to zero molar urea based on the equation

$$\Delta G_{\text{unfold}} = \Delta G_{\text{H}_2\text{O}} - m[\text{urea}] \quad (3)$$

where $\Delta G_{\text{H}_2\text{O}}$ is the free energy unfolding value in the absence of denaturant, [urea] is the molar denaturant concentration, and m is the slope in units of calories per mole per molar.

NMR Spectroscopy. All NMR experiments were performed on a Bruker DRX 600 instrument equipped with a ^1H , ^{15}N , ^{13}C cryoprobe. To detect interactions of NaCl with Ltn10, we performed titration experiments with 100 μM ^{15}N -labeled Ltn in 20 mM sodium phosphate (pH 6) at 283 K. The salt concentration was incrementally increased to 5, 15, 35, 75, 150, 225, and 365 mM NaCl, with subsequent collection of a two-dimensional (2D) ^1H – ^{15}N HSQC spectrum. HSQC cross-peak movements were quantified as a combined ^1H – ^{15}N chemical shift perturbation calculated from

$$\Delta\text{chemical shift} = \sqrt{[(H_o - H) \times 5]^2 + (N_o - N)^2} \quad (4)$$

where H_o and N_o represent reference proton and amide nitrogen parts per million values obtained in starting buffer (0 M NaCl), respectively, and H and N represent proton and amide nitrogen cross-peak parts per million values, respectively, determined at the different NaCl concentrations. Salt binding curves were generated by plotting differences in chemical shift values as a function of NaCl concentration. As NaCl concentrations were increased above 15 mM, chemical shift perturbations were observed for nearly all amide groups, indicating nonspecific interactions across the Ltn10 backbone. As a result, NaCl binding affinities were determined using a ligand interaction model that accounted for nonspecific binding when titration curves appeared to be unsaturable using the equation

$$\Delta\text{CS}_{\text{obs}} = \Delta\text{CS}_{\text{max}} \times \frac{L}{L + K_d} + \text{NS} \times L \quad (5)$$

where $\Delta\text{CS}_{\text{obs}}$ is the observed chemical shift change calculated from eq 4, $\Delta\text{CS}_{\text{max}}$ is the maximal chemical shift difference, L is the ligand concentration (NaCl), K_d is the binding affinity, and NS accounts for nonspecific interactions. Binding affinities were obtained through curve fitting using pro Fit 6.1. When inclusion of the nonspecific interaction term (NS) did not affect the measured K_d value, binding fits were generated using an NS value of zero and are represented as solid lines in Figure 4. In all other instances, titration data displayed unsaturable binding, warranting the use of eq 5 to accurately determine K_d values. Binding fits that include the NS term are represented as dashed lines in Figure 4. The normalized ΔCS was determined from the largest recorded chemical shift difference observed in each titration curve generated

Ltn interconversion rates were determined by 2D longitudinal ^{15}N ZZ-exchange spectroscopy.¹⁶ In these experiments, a series of 2D exchange spectra were acquired with variable mixing times of 50, 150, 200, 250, 300, 350, 400, 500, 750, and 900 ms. Sample conditions consisted of 1 mM Ltn in 20 mM NaH_2PO_4 (pH 6) at 298 K. Comparisons with salt samples were obtained in an identical buffer and at an identical temperature with the addition of 150 mM NaCl. Nonlinear fitting of cross-peak and exchange-peak intensities that accounted for two-site exchange and ^{15}N T_1 relaxation was conducted with an in-house MATLAB 2007b script employing the equations described by Tollinger et al.¹⁷ that allow extraction of k_{for} and k_{rev} Ltn interconversion rates.

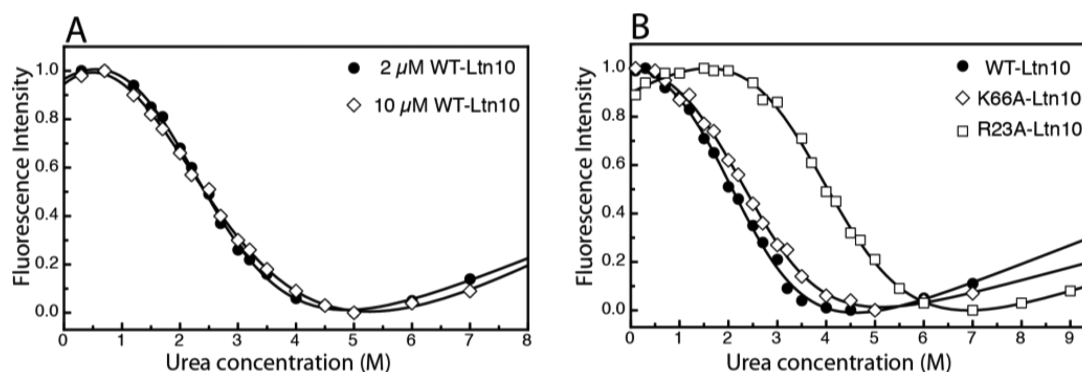


Figure 1. Urea denaturation unfolding curves monitored by fluorescence. (A) Comparison of Ltn unfolding curves collected at 2 and 10 μM in 20 mM Na_2HPO_4 (pH 6) at 25 $^\circ\text{C}$. (B) Unfolding curves for WT and mutant Ltn. All data were obtained with 5 μM protein in 20 mM Na_2HPO_4 (pH 6) at 25 $^\circ\text{C}$. Ltn mutants are denoted with single-letter amino acid abbreviations, followed by the position and the identity of the substitution in the protein sequence. Solid lines connecting data points represent nonlinear fitting to a two-state unfolding model that were included for the sake of clarity and not used in analysis.

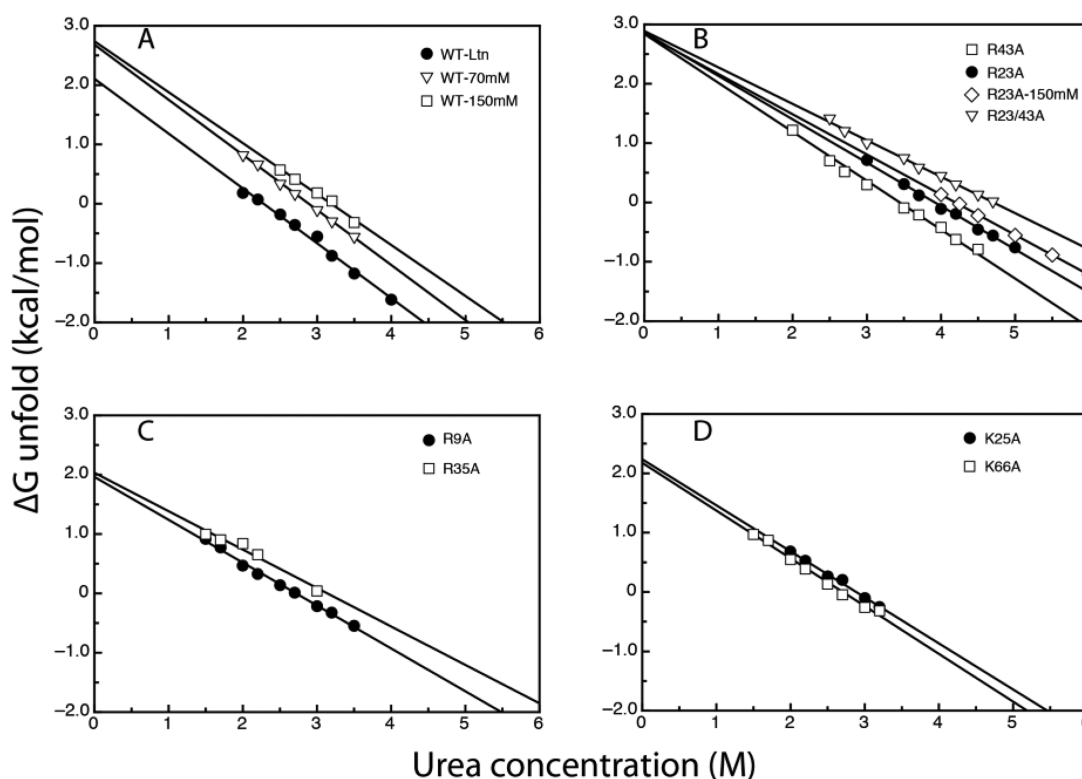


Figure 2. Unfolding free energy (ΔG_{unfold}) of WT and mutant Ltn as a function of urea concentration. All ΔG_{unfold} values were calculated on the basis of eqs 1 and 2, with final extrapolated values determined with eq 3. Experiments conducted in the presence of 70 or 150 mM NaCl in buffer are denoted. (A) Comparison of WT Ltn unfolding values in the absence and presence of NaCl. (B) Comparison of R23A, R43A, and R23/43A Ltn mutants and effect of salt on free energy. (C and D) ΔG_{unfold} vs [urea] for additional arginine and lysine Ltn mutants.

RESULTS AND DISCUSSION

Salt Stabilization of the Ltn10 Conformation. The Ltn structural stability was studied by chemical unfolding at 25 $^\circ\text{C}$ using urea as a denaturant. As Ltn contains only one tryptophan at position 55 (Trp55), the equilibrium unfolding reaction was monitored by measuring the tryptophan fluorescence intensity at 332 nm as a function of urea concentration. To ensure that the fluorescence emission detected was sensitive primarily to monomeric Ltn10 and not a mixture of both structural states, the dependence of the unfolding curve on protein concentration was investigated. It has been shown that the denaturation midpoint for dimeric

proteins is dependent on protein concentration.^{18,19} To assess the contribution of each structural state to fluorescence emission, we collected urea unfolding curves at different Ltn concentrations. We reasoned that if fluorescence emission contained substantial contributions from Ltn40, a characteristic shift in the unfolding curve would be observed. Figure 1A displays unfolding curves generated at different Ltn concentrations indicating that between 2 and 10 μM Ltn protein, the denaturation midpoint is unaffected by protein concentration, which is consistent with fluorescence reporting mainly on the monomeric Ltn10 state. This is not unexpected considering that Trp55 in Ltn10 is buried in the hydrophobic core resulting

in a more intense blue-shifted fluorescence emission spectrum relative to that of dimeric Ltn40, where Trp55 is solvent-exposed.⁷ The baseline WT Ltn10 unfolding value used in our investigation was established at 2 kcal/mol with a 5 μ M protein sample in 20 mM sodium phosphate (Figure 1B), using the linear extrapolation method¹⁵ shown in Figure 2A. To test the effect of NaCl concentration on Ltn10 stability, we conducted additional denaturation experiments in the presence of 70 and 150 mM NaCl. Under both conditions, Ltn10 was stabilized by \sim 1 kcal/mol (Figure 2A and Table 1), indicating that within

Table 1. Ltn10 Unfolding Free Energies Determined for WT and Mutant Constructs^a

Ltn construct	ΔG_{unfold} (kcal/mol)	m value (kcal mol ⁻¹ M ⁻¹)	repulsion pair	distance (Å)
WT	2.1 \pm 0.1	0.92 \pm 0.04	NA	NA
WT ⁷⁰	2.7 \pm 0.1	0.93 \pm 0.02	NA	NA
WT ¹⁵⁰	2.7 \pm 0.2	0.85 \pm 0.06	NA	NA
R9A	2.0 \pm 0.3	0.72 \pm 0.02	R9–K46	10.1 \pm 2.5
R23A	2.9 \pm 0.1	0.73 \pm 0.02	R23–R43	10.1 \pm 2.3
R23A ¹⁵⁰	2.8 \pm 0.1	0.68 \pm 0.01	R23–R43	10.1 \pm 2.3
K25A	2.2 \pm 0.1	0.78 \pm 0.03	K25–R70	5.8 \pm 1.9
R35A	2.0 \pm 0.2	0.65 \pm 0.07	R35–R57	10.5 \pm 1.8
R43A	2.8 \pm 0.1	0.82 \pm 0.03	R23–R43	10.1 \pm 2.3
K66A	2.2 \pm 0.1	0.80 \pm 0.03	K66–K42	5.5 \pm 2.4
R23/43A	3.0 \pm 0.1	0.61 \pm 0.06	R23–R43	10.1 \pm 2.3

^aThe repulsion pair denotes side chain pairs with potentially unfavorable charge–charge interactions that were disrupted by mutation. The distance represents the ensemble average between arginine C ζ or lysine N ζ atoms \pm standard deviation (Protein Data Bank entry 1J8I). The superscript 70 and 150 refer to NaCl concentrations 70 and 150 mM, respectively, used in unfolding experiments. NA means not applicable. The errors in ΔG_{unfold} and m values were estimated from linear fittings using eq 3.

this range, increasing the ionic strength of the environment had a similar effect on Ltn10 stability. We speculated that the observed salt stabilization resulted from a specific interaction rather than a general effect of ionic strength.

Effect of Charge-Change Mutants on ΔG_{unfold} . Given the excess of positive charge carried by Ltn, we reasoned that salt ions might increase stability by weakening repulsive forces within the protein. To differentiate between a general ionic strength effect and a specific NaCl interaction within the Ltn10 structure, a series of charge-change mutants was generated. Mutants were designed to disrupt potentially destabilizing arginine and lysine side chain configurations by alanine substitution. We hypothesized that if the observed salt stabilization was due to nonspecific interactions individual mutations would have little or no effect on fold stability. In contrast, if the increased stability resulted from electrostatic screening of specific repulsive side chain contacts, then mutants at those sites would display a pronounced increase in Ltn10 stability in a manner independent of salt. The free energies of unfolding for six Ltn charge–change mutants were determined by linear extrapolation (Figure 2B–D), with the results listed in Table 1. In the absence of salt, R23A (Figure 1B) and R43A each stabilize the chemokine fold by approximately 1 kcal/mol. Interestingly, introduction of the R23/43A double mutant or addition of 150 mM NaCl to R23A contributed no additional increase in protein stability. Other mutations investigated (i.e., R9A, K25A, R35A, and K66A) showed no significant change in protein stability. Taken together, the free energy analysis is consistent with electrostatic repulsion between Arg23–Arg43 side chains destabilizing the Ltn10 fold, which can be counteracted through increased ionic strength or removal of one of the charged side chains.

Effects of NaCl and Mutations on m Values. The m value, reflected in the slopes of the lines in Figure 2 (listed in Table 1), reports on the dependence of the free energy of

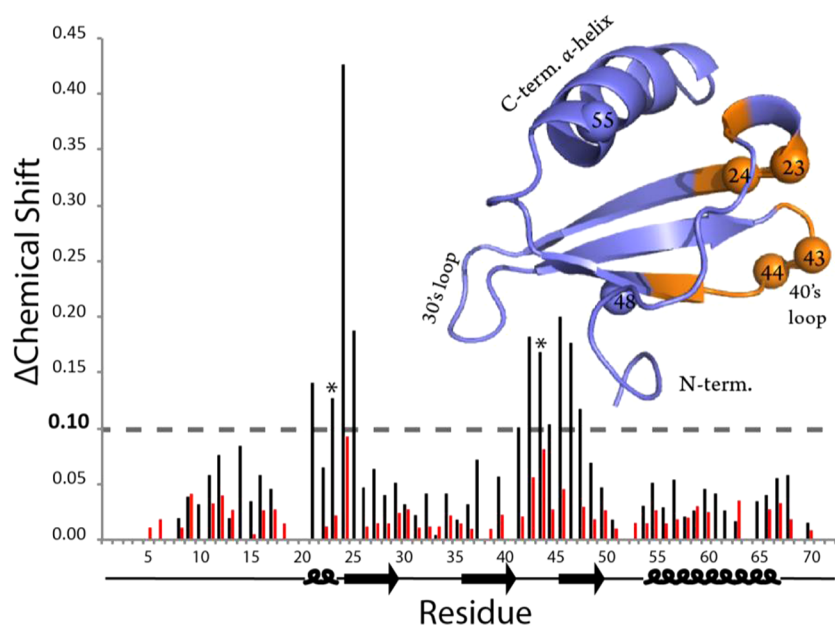


Figure 3. Chemical shift mapping of the interaction of NaCl with the Ltn chemokine fold. The bar plot represents the chemical shift difference (Δ chemical shift) in amide backbone resonances collected at 10 $^{\circ}$ C from 0 and 15 mM NaCl calculated from eq 4, where the asterisks denote the positions of R23 and R43. Residues that displayed Δ CS values of >0.1 ppm are mapped onto the Ltn chemokine fold highlighted in orange. Red bars depict shift perturbations generated using R23A collected at 10 $^{\circ}$ C from 0 and 15 mM NaCl. Spheres shown on the Ltn chemokine structure denote amino acid positions in the primary sequence described in the text.

unfolding on denaturant concentration. Comparisons of m values reveal that within experimental error, addition of 70 or 150 mM NaCl had no significant effect on values observed for WT Ltn10. However all charge-change mutants revealed decreases in the m value relative to that of WT Ltn, with the R23/43A double mutant displaying the largest effect. Decreases in the m value can be indicative of an increased population of intermediate states during protein unfolding or formation of a more compact denatured state;²⁰ however, our data do not allow us to conclusively differentiate between these two possibilities. Considering Ltn unfolding properties, we have not seen evidence of an intermediate state in kinetic unfolding measurements²¹ or observed biphasic denaturation curves (Figure 1). Given the excess of positively charged residues in Ltn, it is possible that removal of Arg or Lys side chains also weakens unfavorable interactions in the denatured state. As changes in the m value have been correlated to differences in the accessible surface area between the folded and denatured states (Δ ASA),²² we speculate that decreases in m values observed for the Ltn mutants may reflect a reduction in Δ ASA resulting from the increased compactness of the denatured states caused by removal of positively charged amino acids.

Identification of a Chloride Ion Binding Site. The interaction between Ltn10 and NaCl was further investigated by ^1H – ^{15}N HSQC spectroscopy. We rationalized that if NaCl binding was mediated through the Arg23 and Arg43 side chains, then salt-induced chemical shift perturbations would localize to this region of Ltn10. In these experiments, ^{15}N -labeled Ltn in 20 mM Na_2HPO_4 (pH 6) was titrated against incremental additions of an identically buffered NaCl solution. All HSQC spectra were collected at 10 °C to ensure that Ltn10 cross-peak movements resulted from a direct interaction with salt ions and not structural interconversion. At a low salt concentration (15 mM), the only significant amide chemical shift perturbations observed (≥ 0.1 ppm) were constrained to areas near Arg23 and Arg43 (Figure 3). The changes in Ltn10 chemical shift values were mapped onto the 3D structure and revealed a specific interaction site that was consistent with a chloride ion binding pocket identified through molecular dynamics simulations.¹³ Interestingly, this same pocket on Ltn was also identified as the binding site for the viral protein M3 chemokine decoy receptor.²³ Considering the composition of residues identified in chemical shift mapping (five positively charged side chains and five hydrophobic side chains), the results are consistent with chloride, rather than sodium ion, acting as the ligand.

To confirm the identity of the R23/R43 chloride recognition site, chemical shift perturbations induced by addition of 15 mM NaCl were monitored for the R23A mutant. Significant salt-induced perturbations (i.e., $\Delta\text{CS} < 0.1$) are no longer observed, indicating that removal of the Arg23 side chain disrupts a specific chloride binding site within the chemokine fold.

Ion Binding Affinity and Selectivity. For the majority of residues identified through chemical shift mapping, binding affinities (K_d) were determined to be approximately 16 mM (Figure 4A), with two outliers displaying values ranging between 40 and 70 mM. Residues outside the revealed binding site displayed much weaker affinities [$K_d > 700$ mM (Figure S1 of the Supporting Information)]. It is difficult to speculate about the discrepancy of these lower affinities, but on the basis of the consensus of data, we estimate a NaCl binding affinity of 16 mM for residues within the region of Arg23 and Arg43. This value appears to be consistent with those of other proteins (e.g.,

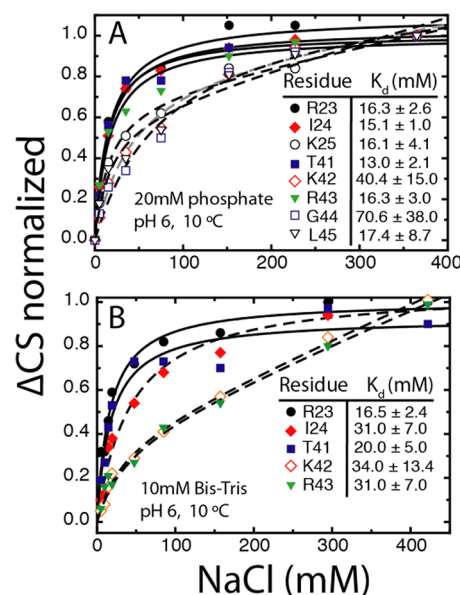


Figure 4. Chloride ion binding curves generated from NMR titration. K_d values were determined by curve fitting to eq 5, with the error estimated from the fitting shown in the inset. Solid and dashed lines representing binding curves denote removal and inclusion of the nonspecific interaction term, respectively, as described in Materials and Methods. (A) NaCl titration curves generated at 10 °C in 20 mM sodium phosphate. (B) NaCl titration curves generated at 10 °C in 10 mM Bis-Tris.

α -amylase and Runx1) known to coordinate chloride ion through arginine and lysine side chains, demonstrating binding affinities between 6 and 34 mM.^{24,25} Considering a K_d value of 16 mM, one expects at physiological concentrations (20 mM phosphate and 150 mM NaCl) ~90% of Ltn10 would have an occupied Arg23/Arg43 binding pocket, with a binding energy of up to 2 kcal/mol. While this exceeds the salt-dependent effect determined by thermodynamic unfolding measurements [WT Ltn10 $\Delta\Delta G \sim 0.6$ kcal/mol (Table 1)], we conclude that a specific interaction at the R23/R43 pocket can easily account for the salt-induced stabilization of Ltn10.

It was demonstrated previously that addition of 10 mM phosphate improved the quality of the 2D NMR spectra of Ltn,²⁶ and we considered the possibility that other anions might bind preferentially to the site detected in our titrations with NaCl that were buffered with 20 mM phosphate. A NaCl titration conducted in 10 mM Bis-Tris buffer (Figure 4B) yielded K_d values for residues located in the Ltn10 chloride binding pocket (Arg23, Ile24, Thr4, and Lys42) that were in good agreement with the values determined in 20 mM phosphate. One notable difference was observed for R43, which required a nonspecific binding term in fitting NaCl titration data in the presence of Bis-Tris (Figure 4B). However, these results indicate that phosphate concentrations at or below 20 mM have a negligible effect on Ltn10–chloride interactions. This does not exclude the possibility of phosphate interacting with the binding pocket, but comparisons of the relative affinity of phosphate and chloride ions (data not shown) indicates that chloride binds preferentially to the R23/R43 site.

Effect of NaCl on Ltn10 Interconversion Kinetics. To further verify the effects of salt on Ltn10 stability, we investigated the dependence of Ltn interconversion rates on NaCl concentration. We reasoned that increasing the stability of Ltn10 would increase the barrier height (ΔG^\ddagger) associated

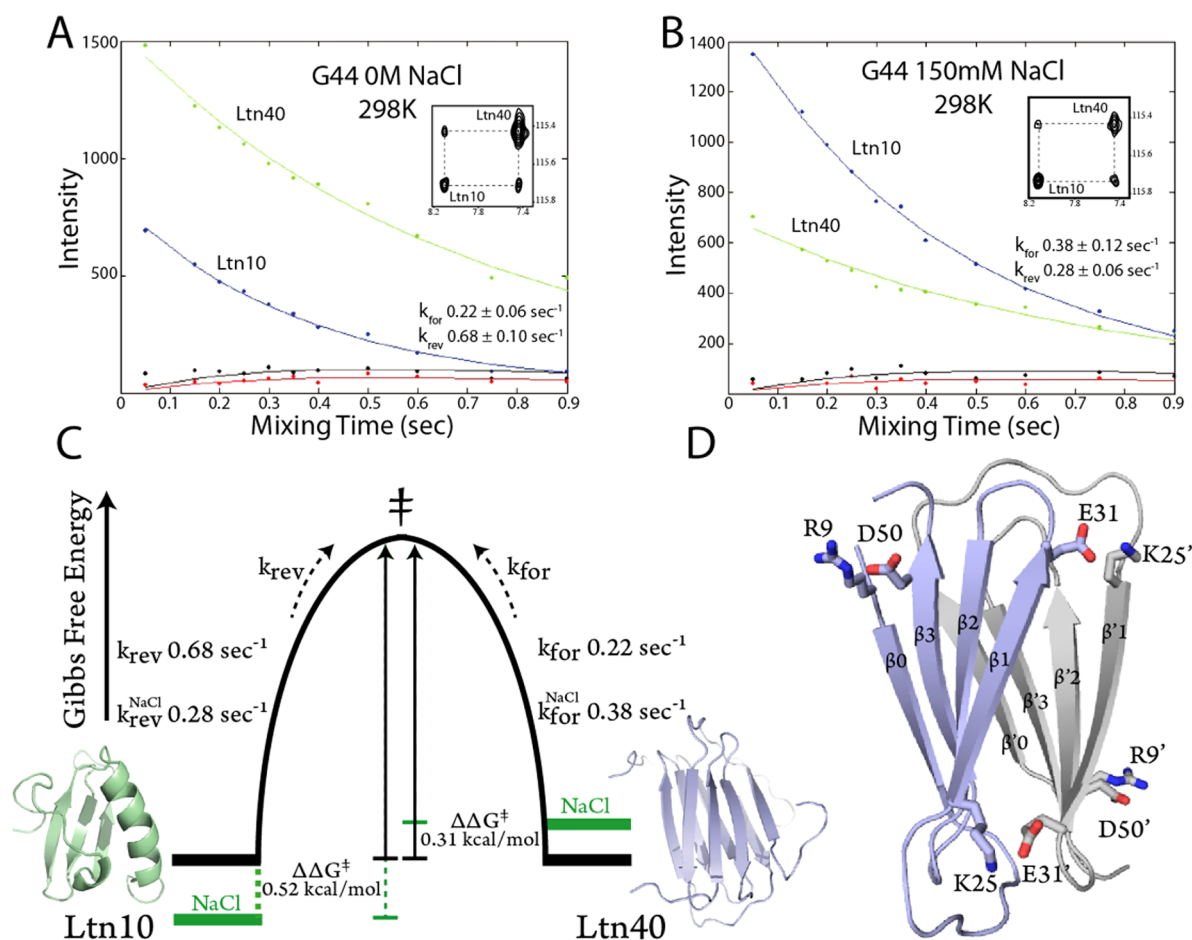


Figure 5. Experimental data and fitted curves for G44 ZZ-exchange. (A) Curves describe the decay of the auto peaks (Ltn10 and Ltn40), with the two bottom curves showing the buildup and decay of exchange peaks in 20 mM Na_2HPO_4 at 25 °C. The inset shows Gly44 cross-peaks for the 750 ms mixing time. (B) Curves describe the decay of the auto peaks (Ltn10 and Ltn40), with the two bottom curves showing the buildup and decay of exchange peaks in 20 mM Na_2HPO_4 and 150 mM NaCl at 25 °C. The inset shows Gly44 cross-peaks for the 750 ms mixing time. (C) Salt dependence of the Ltn free energy landscape. The terms k_{for} and k_{rev} indicate the conversion rate of Ltn as shown by dashed arrows. The NaCl superscript reflects the rate measured in the presence of 150 mM NaCl. $\Delta\Delta G^\ddagger$ values were calculated from the equation described in the text. (D) Intramolecular (R9–D50) and intermolecular (K25–E31) salt bridge interactions found within the Ltn40 dimer.

with structural interconversion and slow the rate at which Ltn10 rearranges to Ltn40 (k_{rev}). Therefore, we determined the effect of NaCl on Ltn interconversion rates (k_{for} and k_{rev}) using ZZ-exchange NMR spectroscopy. A series of 2D exchange spectra were acquired at 25 °C in 20 mM Na_2HPO_4 (pH 6) containing either 0 or 150 mM NaCl employing exchange mixing times ranging from 50 to 900 ms. The ZZ-exchange cross-peak intensities were measured as a function of time (Figure 5A,B), and Ltn interconversion rates were determined by nonlinear fitting using established equations.¹⁷ Measurements involving Gly44 cross-peaks revealed that addition of 150 mM NaCl decreased the Ltn10 → Ltn40 conversion rate (k_{rev}), which is indicated in Figure 5. Additional rates were also determined from Cys48 cross-peak intensities (Figure S2 of the Supporting Information), revealing a similar decrease in k_{rev} values.

Considering the nature of the Ltn energy landscape, it was possible that differences observed in the k_{rev} interconversion rates arose from an increased transition-state free energy as well as stabilization of the Ltn10 conformation. Therefore, we computed the free energy change ($\Delta\Delta G^\ddagger$) reflected in altered k_{rev} rates as $-RT \ln(k_{\text{rev}}/k_{\text{rev}}^{\text{NaCl}})$.²⁷ We reasoned if the free energy changes derived from kinetic measurements were

greater than the energy differences revealed by chemical unfolding, it would support destabilization of the Ltn interconversion transition state. Conversely, if the two values were similar, then any change in kinetics caused by salt could be attributed solely to the protein native state. $\Delta\Delta G^\ddagger$ values of 0.5 kcal/mol determined from ZZ-exchange experiments (Figure 5C) are in excellent agreement with the $\Delta\Delta G$ value of 0.6 kcal/mol derived from Ltn10 urea unfolding experiments (Table 1), and we concluded that an increased ionic strength has little or no effect on the interconversion transition state. This conclusion is consistent with our previous determination that the interconversion transition state is predominately unfolded,²¹ because further destabilization would have been highly unlikely.

Effect of NaCl on Ltn40 Interconversion. As ZZ-exchange spectroscopy reports on the relative stability of each structural conformation at equilibrium, the kinetic measurements also had the potential to detect salt-dependent changes in the free energy of Ltn40. Interestingly, the addition of 150 mM NaCl accelerated the Ltn40 → Ltn10 conversion rate (k_{for}), consistent with a salt-dependent destabilization of the Ltn40 conformation [$\Delta\Delta G^\ddagger \sim 0.3$ kcal/mol (Figure 5)]. Considering the Ltn40 structure, which contains two salt bridge

interactions [e.g., intramolecular from Arg9 to Asp50 and intermolecular from Lys25 to Glu31 (Figure 5D)], this result suggested that increases in the strength of the ionic environment could destabilize the Ltn40 fold through disruption of electrostatic interactions.

Assessing Salt Bridge Contributions to Ltn40 Stability. To assess the energetic contribution of electrostatic contacts within the Ltn40 fold, we determined Ltn10 \leftrightarrow Ltn40 equilibrium constants from ^1H – ^{15}N HSQC peak volumes using the relationship $K_{\text{eq}} = [\text{Ltn40}_{\text{vol}}]/[\text{Ltn10}_{\text{vol}}]$ (Table S1 of the Supporting Information). As noted earlier, the R9A and K25A substitutions have no effect on free energy of unfolding for Ltn10 (Table 1). Thus, we hypothesized that if a specific Coulombic interaction involving either side chain contributed to Ltn40 stability, its disruption would shift the equilibrium toward Ltn10. We found that in the absence of NaCl the K_{eq} of WT Ltn at 25 °C was 1.2 ± 0.2 , consistent with a previous report.¹² Measurements conducted under identical conditions using ^{15}N -labeled R9A and K25A produced K_{eq} values of 1.1 ± 0.5 and 0.40 ± 0.03 , respectively. From these results, we concluded that the Arg9–Asp50 contact has a negligible effect on Ltn40 stability. However, disruption of the intermolecular Lys25–Glu31 salt bridge shifted the equilibrium toward the Ltn10 state, consistent with destabilization of Ltn40 (Figure 5C,D). By comparing the change in K_{eq} values observed for WT and Ltn K25A, we estimate that the Lys25–Glu31 salt bridge contributes ~ 0.6 kcal/mol to Ltn40 stability. While this value is slightly higher than what is expected from ZZ-exchange measurements, this discrepancy may result from the Lys25–Glu31 salt bridge being only partially disrupted in the presence of NaCl, compared to complete removal caused by the K25A mutation.

Conclusions. Our measurements of Ltn thermodynamic stability and interconversion kinetics expand our view into the structural and environmental factors defining its metamorphic folding. Our previous temperature-dependent kinetic investigation was designed to resolve the nature of metamorphic rearrangement, revealing similarities between the transition states associated with protein interconversion and unfolding.²¹ This led us to the perspective that Ltn metamorphosis follows a path resembling protein unfolding and that factors affecting the stability of either native-state conformation can be defined empirically. Here we have identified specific structural elements and environmental factors that optimize the metamorphic folding of Ltn.

This work demonstrates that the Ltn10 fold is destabilized by unfavorable electrostatic interactions between two arginine side chains, which can be counteracted by increasing the ionic strength of the surroundings or specific mutations. These observations support a model in which chloride ion coordination increases the thermodynamic stability of Ltn10 by reducing the local net charge and the extent of Coulombic repulsion between Arg23 and Arg43, slowing the Ltn10 \rightarrow Ltn40 conversion rate. Conversely, a pair of symmetric intermolecular salt bridges that stabilize the Ltn40 structure are weakened in solutions of high ionic strength, increasing the Ltn40 \rightarrow Ltn10 conversion rate. These structural elements appear to balance the relative stabilities of each Ltn conformer, ensuring that both are thermodynamically accessible under physiological conditions of temperature and ionic strength.

We speculate that electrostatic “tuning” of conformational stability may be a common feature in other metamorphic proteins. For example, chloride intracellular channel protein 1

(CLIC1) may also exploit electrostatic interactions in bringing about structural transitions as it inserts into the cell membrane. CLIC1 is a two-domain protein that is comprised of a thioredoxin-like fold (domain 1) and an all- α -helical fold (domain 2). Hydrogen–deuterium-exchange mass spectrometry indicated that the conformational stability of CLIC1 domain 1 is substantially diminished in acidic environments.²⁸ It is suggested that decreased stability results from a reduction in the level of electrostatic attraction caused by protonation of acidic side chains. As CLIC1 approaches the acidic cell membrane, modulation of electrostatic interactions may destabilize the thioredoxin-like domain 1 structure and promote the conversion to a transmembrane helix that inserts into the lipid bilayer.²⁸

Electrostatic effects may also play a contributing role in metamorphic interconversion of the spindle check point protein Mad2 that actively transforms between open and closed states denoted O-Mad2 and C-Mad2, respectively (Protein Data Bank entries 1DUJ and 1S2H, respectively). Conversion of O-Mad2 requires translocation of a C-terminal β -hairpin across the protein while it simultaneously rearranges to form a new β -hairpin with a different hydrogen bonding network.⁶ This transition eliminates potentially unfavorable side chain interactions in O-Mad involving Lys80–Lys113 (~ 7 Å) and Lys161–Lys194 (~ 8 Å) contacts, separating each pair by ~ 20 Å, similar to the Arg23–Arg43 separation achieved by the Ltn10 \rightarrow Ltn40 rearrangement. Transformation into C-Mad2 is completed by the new β -hairpin displacing a short N-terminal β -strand that is incorporated into a central helix. Displacement of the short β -strand appears to require rearrangement of a salt bridge formed between Arg16 and Glu107 that is replaced by a salt bridge between Lys194 and Glu107 upon metamorphic transition. Although the exact role of these residues in Mad2 structural transitions is not known, we speculate that attractive and repulsive electrostatic forces contribute to the Mad2 interconversion process. The available structural and thermodynamic data collectively indicate that metamorphic interconversion can be potentiated by Coulombic forces unique to each native-state conformation.

The existence of metamorphic proteins demonstrates that it is possible to encode more than one ordered structure in a single primary sequence, yet within the framework of the thermodynamic hypothesis, there must exist a balance of free energy between alternate native-state folds that permits structural transition while maintaining energetic equipose. Ltn may provide additional insight into a distinct energy signature that may help better identify metamorphic systems. Considering the energy landscape, we find the relatively shallow well of thermodynamic folding stability observed for Ltn10 (~ 2 – 3 kcal/mol) to be of particular interest, because it permits increased sensitivity to changes in temperature and ionic strength. Moreover, a folded conformation of marginal stability allows greater access to the unfolded state, which is likely required for Ltn structural interconversion.²¹ For example, the folding equilibrium of Ltn10 ($\Delta G_{\text{unfold}} \sim 2$ kcal/mol) populates the unfolded state to a level of $\sim 4\%$. An additional 1 kcal/mol of stability would reduce the unfolded population to 0.6%. In contrast, a typical protein with an unfolding free energy of 4–5 kcal/mol would have a negligible unfolded-state population and a folding equilibrium that is relatively insensitive to a 1 kcal/mol change in ΔG_{unfold} . Thus, marginal thermodynamic stability may be a hallmark of metamorphic proteins that permits access

to the unfolded state and sensitizes the native-state equilibrium to environmental changes.

As more metamorphic proteins are discovered, it will be important to understand the factors that define each native-state structure and govern interconversion. Via identification of unique structural and thermodynamic signatures associated with these systems, it may be possible to encode metamorphic folding into other scaffolds or detect other naturally occurring examples. Molecular switches and reversibly self-assembling nanomaterials with sensitivity to salinity, pH, temperature, or other triggers could be envisioned. The results presented here suggest that electrostatic interactions can be manipulated to direct metamorphic structural transitions, but as more of these systems are elucidated, the rules governing this unique class of proteins will likely expand.

■ ASSOCIATED CONTENT

■ Supporting Information

NMR titration curves generated for residues outside the identified binding site (Figure S1), additional ZZ-exchange data resulting from C48 peak intensities (Figure S2), and details of HSQC peak volumes and K_{eq} values determined for WT and mutant Ltn proteins as described in the text (Table S1). This material is available free of charge via the Internet at <http://pubs.acs.org>.

■ AUTHOR INFORMATION

Corresponding Author

*E-mail: bvolkman@mcw.edu. Phone: (414) 955-8400.

Funding

This work was supported by National Institutes of Health Grant R01 063325.

Notes

The authors declare no competing financial interest.

■ ACKNOWLEDGMENTS

We thank Dr. Evgenii Kovrigin of Marquette University (Milwaukee, WI) for assistance in the analysis of ZZ-exchange data.

■ ABBREVIATIONS

CLIC1, chloride intercellular channel protein 1; HSQC, heteronuclear single-quantum coherence; Mad2, mitotic arrest deficient 2; MD, molecular dynamics; NMR, nuclear magnetic resonance; WT, wild type.

■ REFERENCES

- (1) Anfinsen, C. B. (1973) Principles that govern the folding of protein chains. *Science* 181, 223–230.
- (2) Murzin, A. G. (2008) Biochemistry. Metamorphic proteins. *Science* 320, 1725–1726.
- (3) Bryan, P. N., and Orban, J. (2010) Proteins that switch folds. *Curr. Opin. Struct. Biol.* 20, 482–488.
- (4) Littler, D. R., Harrop, S. J., Fairlie, W. D., Brown, L. J., Pankhurst, G. J., Pankhurst, S., DeMaere, M. Z., Campbell, T. J., Bauskin, A. R., Tonini, R., Mazzanti, M., Breit, S. N., and Curmi, P. M. (2004) The intracellular chloride ion channel protein CLIC1 undergoes a redox-controlled structural transition. *J. Biol. Chem.* 279, 9298–9305.
- (5) Luo, X., Tang, Z., Xia, G., Wassmann, K., Matsumoto, T., Rizo, J., and Yu, H. (2004) The Mad2 spindle checkpoint protein has two distinct natively folded states. *Nat. Struct. Mol. Biol.* 11, 338–345.
- (6) Luo, X., and Yu, H. (2008) Protein metamorphosis: The two-state behavior of Mad2. *Structure* 16, 1616–1625.

- (7) Tuinstra, R. L., Peterson, F. C., Kutlesa, S., Elgin, E. S., Kron, M. A., and Volkman, B. F. (2008) Interconversion between two unrelated protein folds in the lymphotactin native state. *Proc. Natl. Acad. Sci. U.S.A.* 105, S057–S062.
- (8) Kuloglu, E. S., McCaslin, D. R., Markley, J. L., and Volkman, B. F. (2002) Structural rearrangement of human lymphotactin, a C chemokine, under physiological solution conditions. *J. Biol. Chem.* 277, 17863–17870.
- (9) Pace, C. N., and Grimsley, G. R. (1988) Ribonuclease T1 is stabilized by cation and anion binding. *Biochemistry* 27, 3242–3246.
- (10) Courtenay, E. S., Capp, M. W., Saecker, R. M., and Record, M. T., Jr. (2000) Thermodynamic analysis of interactions between denaturants and protein surface exposed on unfolding: Interpretation of urea and guanidinium chloride m-values and their correlation with changes in accessible surface area (ASA) using preferential interaction coefficients and the local-bulk domain model. *Proteins* 4 (Suppl.), 72–85.
- (11) Pegram, L. M., and Record, M. T., Jr. (2008) Thermodynamic origin of hofmeister ion effects. *J. Phys. Chem. B* 112, 9428–9436.
- (12) Volkman, B. F., Liu, T. Y., and Peterson, F. C. (2009) Chapter 3. Lymphotactin structural dynamics. *Methods Enzymol.* 461, 51–70.
- (13) Formanek, M. S., Ma, L., and Cui, Q. (2006) Effects of temperature and salt concentration on the structural stability of human lymphotactin: Insights from molecular simulations. *J. Am. Chem. Soc.* 128, 9506–9517.
- (14) Peterson, F. C., Elgin, E. S., Nelson, T. J., Zhang, F., Hoeger, T. J., Linhardt, R. J., and Volkman, B. F. (2004) Identification and characterization of a glycosaminoglycan recognition element of the C chemokine lymphotactin. *J. Biol. Chem.* 279, 12598–12604.
- (15) Shirley, B. A. (1995) Urea and guanidine hydrochloride denaturation curves. *Methods Mol. Biol.* 40, 177–190.
- (16) Farrow, N. A., Zhang, O., Forman-Kay, J. D., and Kay, L. E. (1994) A heteronuclear correlation experiment for simultaneous determination of ^{15}N longitudinal decay and chemical exchange rates of systems in slow equilibrium. *J. Biomol. NMR* 4, 727–734.
- (17) Tollinger, M., Skrynnikov, N. R., Mulder, F. A., Forman-Kay, J. D., and Kay, L. E. (2001) Slow dynamics in folded and unfolded states of an SH3 domain. *J. Am. Chem. Soc.* 123, 11341–11352.
- (18) Bowie, J. U., and Sauer, R. T. (1989) Equilibrium dissociation and unfolding of the Arc repressor dimer. *Biochemistry* 28, 7139–7143.
- (19) Maity, H., Mossing, M. C., and Eftink, M. R. (2005) Equilibrium unfolding of dimeric and engineered monomeric forms of lambda Cro (F58W) repressor and the effect of added salts: Evidence for the formation of folded monomer induced by sodium perchlorate. *Arch. Biochem. Biophys.* 434, 93–107.
- (20) Hammack, B., Attfield, K., Clayton, D., Dec, E., Dong, A., Sarisky, C., and Bowler, B. E. (1998) The magnitude of changes in guanidine-HCl unfolding m-values in the protein, iso-1-cytochrome c, depends upon the substructure containing the mutation. *Protein Sci.* 7, 1789–1795.
- (21) Tyler, R. C., Murray, N. J., Peterson, F. C., and Volkman, B. F. (2011) Native-state interconversion of a metamorphic protein requires global unfolding. *Biochemistry* 50, 7077–7079.
- (22) Myers, J. K., Pace, C. N., and Scholtz, J. M. (1995) Denaturant m values and heat capacity changes: Relation to changes in accessible surface areas of protein unfolding. *Protein Sci.* 4, 2138–2148.
- (23) Alexander-Brett, J. M., and Fremont, D. H. (2007) Dual GPCR and GAG mimicry by the M3 chemokine decoy receptor. *J. Exp. Med.* 204, 3157–3172.
- (24) Feller, G., Bussy, O., Houssier, C., and Gerday, C. (1996) Structural and functional aspects of chloride binding to *Alteromonas haloplantis* α -amylase. *J. Biol. Chem.* 271, 23836–23841.
- (25) Wolf-Watz, M., Backstrom, S., Grundstrom, T., Sauer, U., and Hard, T. (2001) Chloride binding by the AML1/Runx1 transcription factor studied by NMR. *FEBS Lett.* 488, 81–84.
- (26) Marcaurelle, L. A., Mizoue, L. S., Wilken, J., Oldham, L., Kent, S. B., Handel, T. M., and Bertozzi, C. R. (2001) Chemical synthesis of lymphotactin: A glycosylated chemokine with a C-terminal mucin-like domain. *Chemistry* 7, 1129–1132.

- (27) Gardino, A. K., Villali, J., Kivenson, A., Lei, M., Liu, C. F., Steindel, P., Eisenmesser, E. Z., Labeikovsky, W., Wolf-Watz, M., Clarkson, M. W., and Kern, D. (2009) Transient non-native hydrogen bonds promote activation of a signaling protein. *Cell* 139, 1109–1118.
- (28) Stoychev, S. H., Nathaniel, C., Fanucchi, S., Brock, M., Li, S., Asmus, K., Woods, V. L., Jr., and Dirr, H. W. (2009) Structural dynamics of soluble chloride intracellular channel protein CLIC1 examined by amide hydrogen-deuterium exchange mass spectrometry. *Biochemistry* 48, 8413–8421.